Tuned and screened range-separated hybrid density functional theory for describing electronic and optical properties of defective gallium nitride

D. Kirk Lewis,[1] Ashwin Ramasubramaniam,[2] and Sahar Sharifzadeh[1,3,*]

[1]*Department of Electrical and Computer Engineering, Boston University, Boston, Massachusetts 02215, USA*
[2]*Department of Mechanical and Industrial Engineering, University of Massachusetts Amherst, Amherst, Massachusetts 01003, USA*
[3]*Division of Materials Science and Engineering, Boston University, Boston, Massachusetts 02215, USA*

(Received 27 March 2020; accepted 11 May 2020; published 18 June 2020)

We apply a hybrid density functional theory approach, based on a tuned and screened range-separated hybrid (SRSH) exchange-correlation functional, to describe the optoelectronic properties of defective gallium nitride (GaN). SRSH and time-dependent SRSH (TDSRSH) are tuned to produce accurate energetics for the pristine material and applied to the study of a series of point defects in bulk GaN, a blue light-emitting material that degrades in the presence of defects. We first establish the accuracy of the method by comparing the predicted quasiparticle gap and low-energy excitation spectra of (TD)SRSH and many-body perturbation theory for both pristine GaN and GaN containing a single nitrogen vacancy. Aided by the reduced computational cost of (TD)SRSH, we then report on three additional technologically relevant point defects and defect complexes in GaN: the gallium vacancy, the carbon interstitial, and the carbon-silicon complex. We compute the low-energy optical absorption spectra for these defects and show the presence of defect-centered transitions. Furthermore, by estimating the Stokes shift, we predict, in agreement with previous studies, that the carbon substitutional defect is a candidate for the detrimental yellow luminescence in GaN. This study indicates that TDSRSH is a promising and computationally feasible approach for quantitatively accurate, first-principles modeling of defective semiconductors.

DOI: 10.1103/PhysRevMaterials.4.063803

I. INTRODUCTION

Defects in semiconductors play a pivotal role in devices because they can dominate the optoelectronic response of materials [1]. Defects can lead to carrier trapping sites that decrease carrier lifetimes and limit conductivity [2–4] and can also localize optical excitations, altering their energetics and excitonic properties [5–7]. Thus, it is essential to characterize precisely the electronic structure associated with particular defects.

Due to the difficulty of unequivocally relating experimentally measured defect energetics to defect identity, first-principles theory has made vital contributions to understanding the influence of defects in important semiconductors where they play a role (e.g., Si, GaAs, GaN) [8–22]. In particular, density functional theory (DFT) has predicted qualitatively, and even sometimes quantitatively, accurate thermodynamic transition levels induced by point defects [23,24]. Additionally, configuration coordinate diagrams constructed from DFT calculations can accurately predict absorption and photoluminescence properties of defective semiconductors when transitions result in a change of the defect charge state (i.e., the transition is to/from a bulklike state from/to a defectlike state) [23,24]. However, an open problem remains as to how accurate, yet computationally feasible, absorption and emission properties may be calculated for general defect transitions in solids, including excitonic effects. This is especially important for applications that rely on defect-defect transitions [25,26].

There have been limited DFT-based studies that can probe defect-defect optical transitions. For example, constrained DFT (CDFT) has been used to describe the energetics and Stokes shift of defect-defect transitions within the NV center in diamond [27,28]. This approach is reliable if, among other conditions, the excited state can be described by a single Slater determinant [25]. Time-dependent DFT (TDDFT) does not in principle suffer from this limitation and does not require an *a priori* assumption regarding the nature of transitions. TDDFT has been applied to predict transition energies, optical absorption, exciton binding energies, and nonradiative recombination rates in defective materials (e.g., [29–31]). However, a description of excitonic effects in solids requires an exchange-correlation functional that captures long-range Coulomb interactions [32], that are lacking in standard DFT functionals as well as some hybrid DFT functionals.

Many-body perturbation theory (MBPT) within the *GW* approximation [32–39] and the Bethe-Salpeter equation (BSE) approach [32,38–41] is the current state-of-the-art approach for quantitatively accurate first-principles prediction of (opto)electronic properties in the solid state. MBPT has been applied to a limited extent to the study of defects in semiconductors (e.g., Refs. [29,42–62]). However, the high computational cost of MBPT motivates the use of methods, often based on hybrid DFT functionals (e.g., HSE [63,64] or PBE0 [65]), that are more accurate than DFT yet affordable

*ssharifz@bu.edu

relative to MBPT. Screened range-separated hybrid (SRSH) DFT [66–81] is one such promising method. This approach falls within generalized Kohn-Sham theory [82], with the added constraint that, in the long range, the functional should behave as a screened Coulomb potential. Importantly, because of the long-range nature of the SRSH functional, it can describe excitonic effects in solids [32,67]. Tuned SRSH functionals, for which the range-separation and solid-state screening parameters are fit to each material specifically, have been shown to produce accurate band structures and optical absorption spectra for a range of solids, including organic solids, and bulk and two-dimensional (2D) inorganic materials (e.g., [69,70,79,83–85]). Such a method could potentially allow for the study of the multitude of defect states present in real materials, for which MBPT is computationally prohibitive, with quantitative accuracy. For select two-dimensional materials with weak screening, unscreened RSH [86] and screened SRSH [30] have been utilized to predict defect energetics. However, the accuracy of TDSRSH, which accounts for the significant bulk screening, has not been established for describing the energetics of defects in semiconductors.

Here, we apply tuned SRSH to study a series of point defects and a defect complex within bulk GaN, a technologically important and well-studied material, which naturally contains such point defects [24,87,88]. GaN is a prominent blue light-emitting diode material, known to degrade into a yellow or green color due to the presence of defects. The nature of all the defects that may lead to yellow or green luminescence (YL, GL) is not yet known with certainty [89]. We first establish the accuracy of our SRSH method by comparison to *GW*/BSE calculations on the pristine bulk and on bulk GaN containing a nitrogen vacancy in the 1+ charge state (V_N^{1+}). We then proceed to study a series of defects, determining the nature and energy of the transitions. Specifically we study a charged Ga vacancy (V_{Ga}^{3-}), a charged carbon substitutional defect (C_N^{1-}) and the carbon-silicon substitutional complex (C_N-Si_{Ga}). All four defects studied have been suggested to play an important role in the behavior of GaN as an LED or power electronic material [19,22,90–96]. We predict, in agreement with previous theoretical studies [19] and experiment [96], that the carbon impurity is a candidate for YL. Our results are important in that they represent one of the first calculations of optical absorption properties of defective GaN, while also establishing the viability of the (TD)SRSH approach for quantitatively accurate modeling of defects in semiconductors.

II. COMPUTATIONAL DETAILS

A. Density functional theory

DFT and TDDFT calculations were performed within the VASP package [97] with core electrons and nuclei described by the projector-augmented wave method (PAW) [98]. We studied pristine bulk GaN and four technologically important defects: the V_N^{1+}, V_{Ga}^{3-}, C_N^{1-}, C_N-Si_{Ga}. Initial structures for pristine and with-defect GaN were obtained from previous DFT calculations when possible [21,99]. We obtained the GaN unit-cell vectors and the structure of V_N^{1+} from Ref. [99] and the V_{Ga}^{3-} and C_N^{1-} structures from Ref. [21]. For the C_N-Si_{Ga} defect, we optimized the geometry within the VASP package in a way that is consistent with these previous studies. The relaxations were performed within collinear spin-polarized DFT with Ga *d* electrons explicitly included as valence. The lattice vectors of the close-packed hexagonal wurtzite GaN unit cell were 3.20 Å along the *a* and *b* axes and 5.2 Å along the *c* axis, in good agreement with experiment [100]. From this geometry, a 4×4×3 supercell was constructed (see Fig. 1), a defect was introduced into the supercell, and the geometry was reoptimized in the presence of the defect using the HSE functional [101] with 30% exact exchange, which was the amount necessary to match the GaN experimental band gap of 3.5 eV [102]. The calculations were performed with a plane-wave cutoff energy of 425 eV, and a Monkhorst-Pack (MP) *k* mesh [103] of 8×8×8 (2×2×2) for the unit (super) cells. All geometry relaxations used a Γ-centered *k*-point mesh except for the V_N^{1+} supercell obtained from previous work [99] where the *k* mesh was shifted off Γ to reduce defect-defect interaction [104]. The structure was relaxed until forces were less than 0.05 eV/Å and total energy change was less than 1×10^{-4} eV.

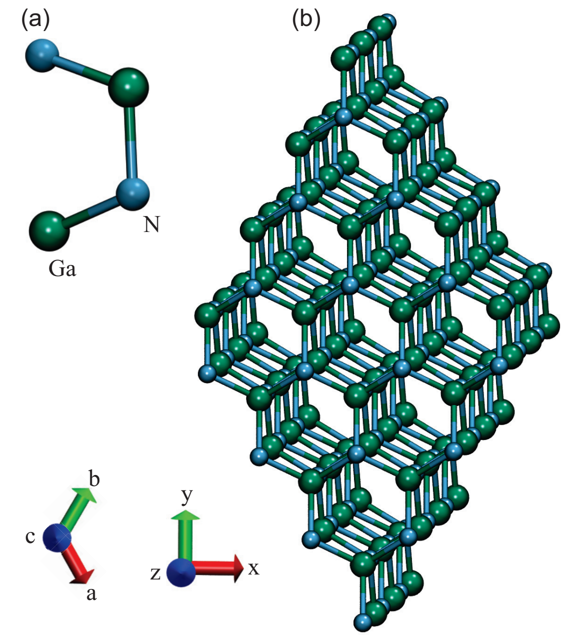

FIG. 1. The structure of bulk wurtzite GaN. (a) Shows the pristine unit cell and (b) the 4×4×3 192-atom supercell for defect studies.

DFT band structure and TDDFT calculations were performed within VASP using PAW potentials that include only the Ga 4*s* and 4*p* electrons as valence. For band structure calculations of the unit cell, the Kohn-Sham orbital energies were interpolated to the *k*-point path using maximally localized Wannier functions [105] via the WANNIER90 software package [106]. For SRSH and TDSRSH calculations, we utilized a customized version of the VASP package as implemented by prior work [79,85].

The SRSH functional contains three fitting parameters: (1) the fraction of exact short-range exchange; (2) the range-separation parameter beyond which the exchange-correlation functional is set to the exact exchange screened by the dielectric constant; and (3) the dielectric constant. Previous studies determining these parameters either from first principles or empirically have shown that *GW* eigenvalues and BSE optical spectra can be reproduced by SRSH and TDSRSH, respectively [69,70,79,83–85]. In this work, the SRSH hybrid was tuned according to the procedure of Ref. [70]; the fraction of short-range exchange was set to 0.25; the range-separation parameter was set to 0.70 Å^{-1}, tuned to match the pristine unit-cell band gap to the experimental value 3.50 eV [102]; and the dielectric constant was set to $5.4\epsilon_0$ (where ϵ_0 is the vacuum permittivity) as calculated within the random phase approximation (RPA) [107,108]. When using the HSE functional the amount of exact exchange was tuned to 30% in order to match the experimental band gap. The ground-state wave functions were calculated on a $16\times16\times16$ Γ-centered MP *k*-point mesh for the pristine unit cell and $4\times4\times4$ Γ-centered MP mesh for the defective supercell, and the dielectric matrix was calculated on the respective *k*-point grid, neglecting local field effects [109]. To better understand the potential of the C_N^{1-} defect as the source of yellow luminescence, we additionally studied this defect with a denser $8\times8\times8$ *k*-point mesh. Subsequently, we solved the Casida equations [110] to obtain the optical spectrum and the exciton energies of the materials with 12 valence and 7 conduction bands for the defective supercell, and 6 valence and 6 conduction bands for the pristine unit cell. To describe the nature of optical transitions, we calculated the density associated with the electron and hole as shown in Fig. 5 as a linear combination of excitations from/to occupied/unoccupied Kohn-Sham orbitals, weighted by the square of the coefficients obtained from solving the TDDFT Casida equation.

B. Many-body perturbation theory

GW/BSE calculations were performed on both the GaN unit cell and the V_N^{1+} defect supercell as outlined in Refs. [7,99]. We calculated optical absorption using the BERKELEYGW software package [111] with starting DFT orbitals obtained from the QUANTUM ESPRESSO software package [112]. The BSE sum was expanded over 12 and 7 (8 and 6) conduction and valence bands, respectively, for the supercell (unit cell). The BSE kernel was interpolated from a *k* mesh of $2\times2\times2$ ($8\times8\times8$) to $4\times4\times4$ ($16\times16\times16$) for the supercell (unit cell). The Ga 4*s*4*p* electrons were included as valence. To generate the *GW* band structure for the unit cell, the quasiparticle corrections were interpolated from the coarse *k* mesh to the *k*-point path using the BERKELEYGW software package [111]. Further details of the *GW*/BSE calculations are contained in previous studies [7,99].

C. Defect-defect interaction corrections

For charged defects, we must apply a post-self-consistent-field correction to the defect-localized state energies to correct for the artificial interaction of a charged defect with its periodic images [48,113]. This correction can be approximated as,

$$\epsilon_{d,\mathrm{corr}} = -\frac{2}{q}E_{\mathrm{corr}}, \tag{1}$$

TABLE I. Defect-state electrostatic correction energies obtained from Eq. (1). The C_N-Si_{Ga} defect was studied in the neutral charge state; hence, no correction was required.

Defect	$\epsilon_{d,\mathrm{corr}}$ (eV)
V_N^{1+}	−0.272
V_{Ga}^{3-}	1.025
C_N^{1-}	0.358

where q is the charge state of the defect and E_{corr} is the electrostatic correction to the total energy of the charged defect supercell [114,115] obtained from Refs. [21,22]. The electrostatic corrections applied to defect-state energies are given in Table I.

We identify the defect-localized bands that require the correction by calculating the radial expectation value of the Kohn-Sham orbitals per Ref. [99],

$$\langle r\rangle = \frac{\int \|\mathbf{r}-\mathbf{r}_d\|\rho(\mathbf{r})d^3r}{\int \rho(\mathbf{r})d^3r}, \tag{2}$$

where $\mathbf{r}_d$ is the center of mass of a state's electron charge density (see Ref. [116]). For each Kohn-Sham orbital at each *k* point considered, $\langle r\rangle$ is calculated. The radial expectation value for localized defect states is significantly smaller than that for extended bulklike states, and so the defect-localized states are easily identifiable. The electron density used in Eq. (2) is computed for each band as a weighted average over all *k* points. The corrected DFT state energies are used in the reported SRSH orbital energies and incorporated into the TD-SRSH starting point. For the latter, we input these corrected eigenvalues into the VASP wave-function file (WAVECAR) using a custom script as described in Ref. [116].

While the electrostatic correction can account for some defect-defect interactions, the limited size of the supercell results in a residual defect-defect interaction which gives a dispersion of the defect-state energies [99]. Thus, when reporting defect-state energies in band-diagram format, we calculate the weighted average over the *k* mesh per Ref. [117]:

$$\overline{E_d^C} = \frac{\sum_N w_N E_d^C(N)}{\sum_N w_N}, \tag{3}$$

where $E_d^C(N)$ is the energy of a particular defect state at a particular *k* point, w_N is the associated *k*-point weight and N runs over all *k* points.

III. RESULTS

A. Comparison of *GW*/BSE, TDSRSH, and TDHSE

We first present a comparison of the different levels of theory considered [*GW*/BSE, (TD)HSE, and (TD)SRSH] for predicting the band structure and optical properties of pristine GaN. For the band structure, as shown in Fig. 2(a), there is an excellent agreement between the different levels of theory. The band gap agrees to within 0.04 eV and the mean absolute error (MAE) in the band dispersion relative to the *GW* results, over the *k* path and energy range shown in Fig. 2(a) is 0.13 eV for DFT-HSE and 0.11 eV for DFT-SRSH. The line shapes

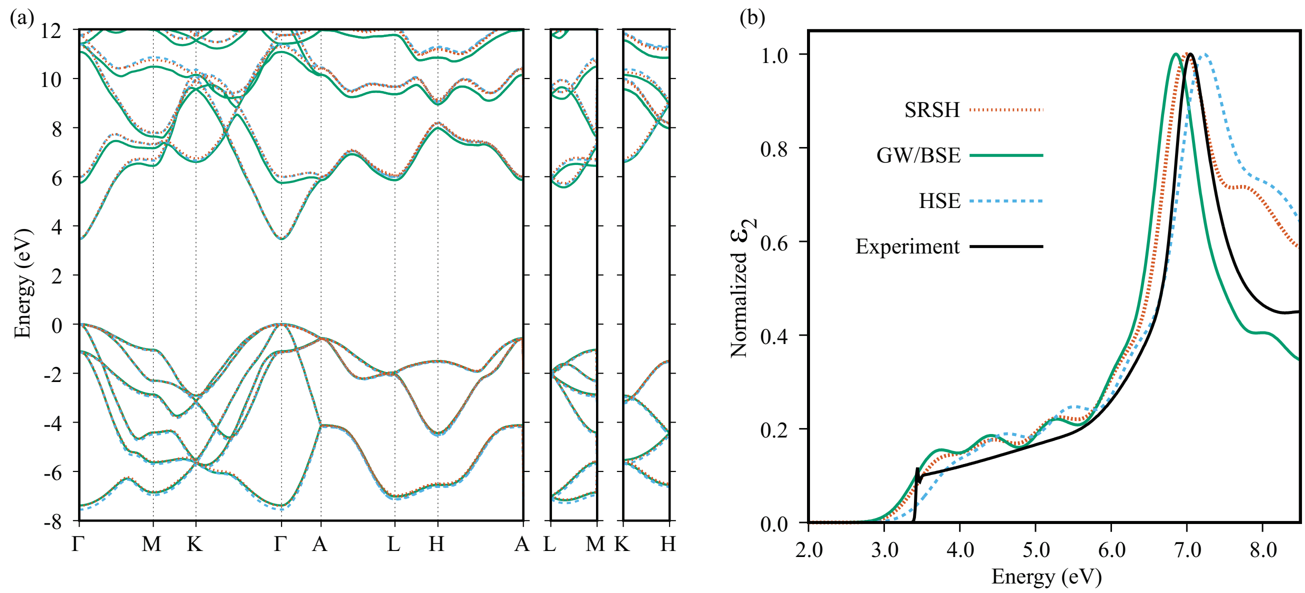

FIG. 2. (a) Band structure within *GW*, DFT-HSE, and DFT-SRSH and (b) imaginary component of the dielectric function within *GW*/BSE, TDHSE, and TDSRSH for pristine GaN. In (a) the band structure path for a hexagonal lattice from Ref. [119] was used. For (b) a broadening of 0.25 eV was applied to the theoretical results to mimic experimental broadening and the spectra were normalized such that the highest peak position is at 1. The experimental dielectric function is taken from Ref. [118].

of the imaginary part of the dielectric function for bulk GaN as shown in Fig. 2(b), agree as well, though there is a more significant discrepancy in peak energies. The best agreement with the position of the experimental absorption [118] peak at approximately 7.05 eV is obtained with the SRSH functional (7.0 eV); BSE slightly underestimates the peak's position at 6.86 eV while TDHSE overestimates it at 7.88 eV. *GW*/BSE appears to best reproduce the overall shape of the measured absorption response in the shown energy window of 2–8 eV; TDHSE and TDSRSH show a similar line shape but display a shoulder at energies higher than the main peak that is not present in the measured spectrum. All predicted spectra display small oscillations in the absorption response from the onset to approximately 6 eV. This feature is not observed in measurement and may be due to an undersampling of the k-point mesh or lack of incorporation of finite-temperature effects in the theory which would broaden and smooth the spectrum.

TABLE II. Absorption onset and exciton binding energy of pristine and defective GaN obtained from *GW*/BSE, TDSRSH, and TDHSE.

Method	Absorption onset (eV)	E_b (meV)
Pristine bulk (unit cell)		
BSE	3.34	120
TDSRSH	3.33	140
TDHSE	3.45	2
GaN containing one V_N^{1+} point defect (4×4×3 supercell)		
BSE	3.33	130
TDSRSH	3.45	156
TDHSE	3.58	3

As shown in Table II, the onset of absorption agrees to within 12 meV for all levels of theory. The predicted exciton binding energy is ∼5 times larger than the experimental value of ∼25 meV [120] for BSE and TDSRSH and ∼13 times smaller for TDHSE. The near-zero value from TDHSE may be due to the fact that the exchange-correlation kernel lacks a nonlocality in the long range (i.e., $q \to 0$), which has been shown to be necessary to fully describe excitonic effects in solids [32]; TDHSE has been shown to partially capture these effects [121]. The discrepancy of the BSE and TDSRSH predicted binding energies when compared with experiment can be understood as being due to a lack of k-point convergence; the k-point dependence of the binding energy has been shown to be quite significant, requiring a large k-point mesh near Γ [6,81,122]. Here, we estimate an error of ∼0.1 eV in the exciton binding energy and, thus, the optical absorption onset, due to the limited k-point sampling.

To further understand the accuracy of TDHSE and TDSRSH, we compute the defect-induced electronic states and optical absorption spectrum of GaN containing one nitrogen defect in the 1+ charge state (V_N^{1+}) and compare to *GW*/BSE. When compared with the *GW* approximation, the predicted defect-centered electronic state energies agree to within 0.14 eV for SRSH and 0.2 eV for HSE (see Table S1 in Ref. [116]). Considering that we estimate a ∼0.1 eV level of accuracy for *GW*, these agreements are quite good. As shown in Fig. 3 and Table II, there is a discrepancy between the onset of absorption for the different levels of theory, as with pristine GaN, with TDSRSH and *GW*/BSE in better agreement than with TDHSE. While the shapes of the *GW*/BSE and TDSRSH spectra over the displayed window of 2–5 eV are similar, they are qualitatively different from the TDHSE result: the TDHSE spectrum shows three peaks of approximately equal amplitude as opposed to the single dominant peak of the *GW*/BSE and TDSRSH spectra.

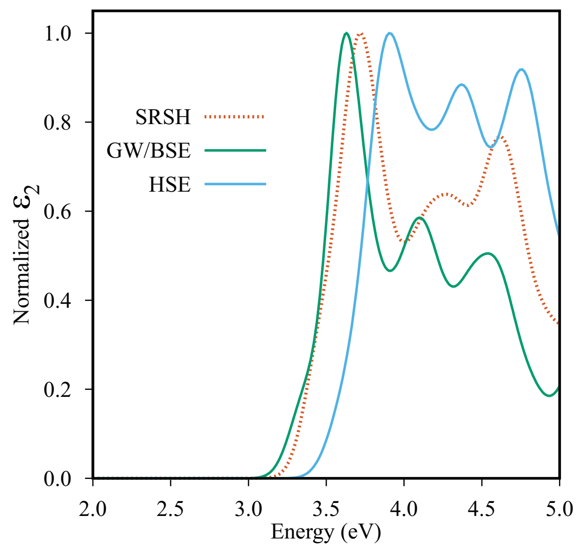

FIG. 3. Predicted imaginary component of the dielectric function for GaN containing one V_N^{1+} defect for BSE, TDSRSH, and TDHSE. For these calculations, no electrostatic correction has been applied to defect-state energies.

The discrepancy in the absorption onset between *GW*/BSE and the TDDFT calculations is somewhat larger in the presence of the defect (see Table II). However, TDSRSH and *GW*/BSE still agree to 0.12 eV with predicted onset energies of 3.45 and 3.33, respectively. The TDHSE predicted onset is 0.25 eV larger than *GW*/BSE at 3.58 eV. Additionally, the exciton binding energies predicted by TDSRSH and BSE agree to within 26 meV, while the value predicted by TDHSE is more than 40 times smaller than either the *GW*/BSE. We note that in the presence of the defect, the predicted binding energies from *GW*/BSE, TDSRSH, and TDHSE are all quite similar to their pristine values. We expect a similar under-convergence with respect to *k*-mesh sampling and estimate a ~0.1 eV uncertainty in the onset of absorption.

B. SRSH-computed trap-state energies and optical spectra for a series of point defects

As shown above, (TD)SRSH quantitatively reproduces both the energetics and absorption line shape of *GW*/BSE at a significantly reduced computational cost, and is thus a promising approach for studying how defects influence the optical absorption spectrum of GaN. Here, we present the defect-state trap energies and GaN optical absorption spectra in the presence of a series of point defects: V_N^{1+}, V_{Ga}^{3-}, C_N^{1-}, and C_N-Si_{Ga}, along with transition state analyses. All four defects have been suggested to play an important role in the behavior of GaN as an LED or power electronic material. The nitrogen vacancy, which may occur in *p*-doped GaN due to its low formation energy [21,94,123], has been suggested as potentially contributing to both the YL at an energy of ~2.18 eV [94] and the GL2 band at 2.33 eV [95]. The gallium vacancy, with a relatively low formation energy in *n*-type GaN [21], may play a role in the YL as well [90,91,124]. Recent measurements [96] indicate that the carbon impurity, which also has a low formation energy in *n*-type GaN, is responsible for the observed YL1 band at ~2.17 eV, a conclusion that is supported by theory [19,92]. Lastly, the carbon-silicon defect complex C_N-Si_{Ga} can have a relatively small formation energy, especially in Ga-rich material and has been associated with an observed trap state [22,93]. Here, we investigate the optoelectronic properties of each defect.

The band diagrams associated with these defective crystals [Figs. 4(a)–4(d)] show that there are multiple localized states associated with each point defect studied. The bulk GaN band gap is predicted to be 3.46–3.6 eV within these supercells. This value is different from pristine GaN because of the perturbation due to the presence of a periodically repeating defect. With introduction of V_N^{1+}, there are four localized states introduced by the defect: one fully occupied below the valence band maximum and three unoccupied states within the conduction band [99]. Thus, the band gap is approximately unchanged. With V_{Ga}^{3-}, four localized states are introduced deep in the band gap, with all four being fully occupied. This results in a significant lowering of the effective gap to 1.27 eV. Similarly, for C_N^{1-}, there are three mid-gap defect states, all fully occupied, resulting in lowering of the effective band gap to 2.83 eV. The C_N-Si_{Ga} defect has a lesser effect on the gap, with two occupied defect-localized states near the valence band maximum: one just above and another just below the band edge, reducing the effective gap to 3.46 eV.

The electronic transitions associated with the V_N^{1+}, V_{Ga}^{3-}, C_N^{1-}, and C_N-Si_{Ga} defect-centered states result in modification of the imaginary component of the dielectric function in a way that follows trends in the band diagram. As shown in Fig. 4(e), the nitrogen vacancy only weakly modifies the absorption spectrum relative to the pristine material. This is expected because the defect-centered states for this defect are nearly degenerate with bulklike states. In contrast, V_{Ga}^{3-} defect strongly modifies the absorption spectrum for a broad range of energies below the pristine material's absorption onset. In particular, there are now two low-energy peaks located at 1.6 and 2.3 eV with absorption strength of ~20% and ~15%, respectively, of the bulklike low-energy peak at 3.7 eV. The introduction of the C_N^{1-} defect also has a major impact on the absorption spectrum with a peak at approximately 3.0 eV and absorption strength ~40% of the bulklike peak. We predict that introduction of C_N-Si_{Ga} results in minor changes to the absorption spectrum: the main impact appears to be a slight shift of the onset to lower energy.

The nature of the lowest-energy transition as calculated from TDDFT is shown in Fig. 5, which again follows the band diagram of Fig. 4. For V_N^{1+}, the lowest-energy transition is a bulk-to-bulk transition.[1] For all other defect states, the lowest-energy excited state is a defect-to-bulk transition, consistent with Fig. 4. In all cases, the orbital associated with the electron is a delocalized bulklike state of *s* symmetry

[1]We note that the character of the transition for V_N^{1+} is different than the *GW*/BSE data presented in Ref. [7], where a bulk to defect lowest-energy transition was predicted. This is because the bulk and defect-state energies are degenerate in the conduction band and so their ordering is highly sensitive to the *k*-point mesh. Reference [7] used a *k*-point mesh shifted off of Γ in order to minimize defect-defect interactions.

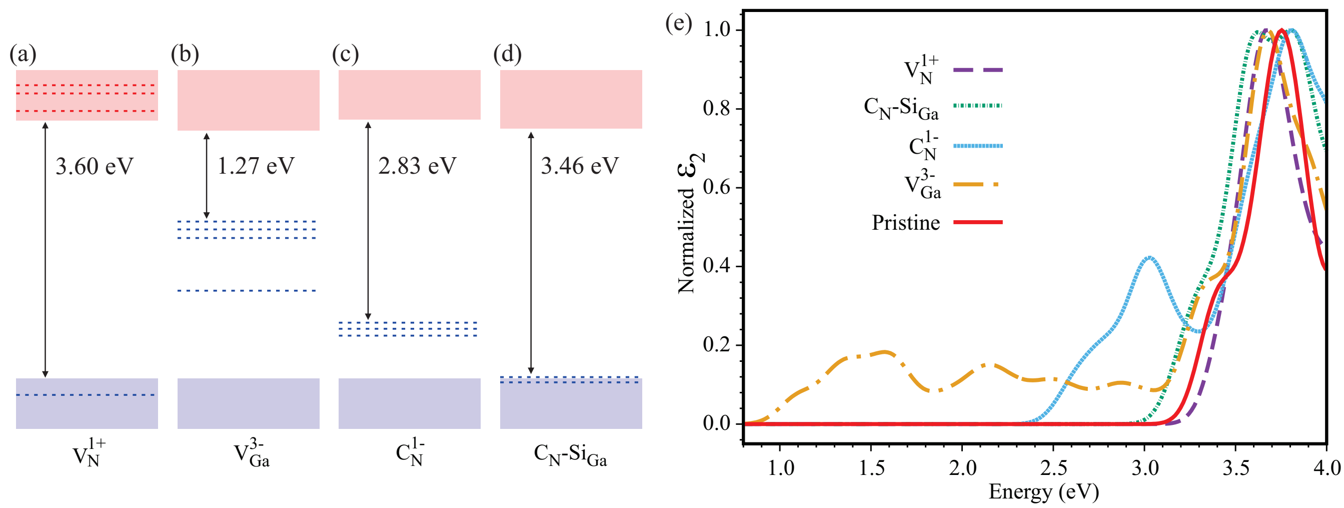

FIG. 4. Band diagram for GaN in the presence of the (a) V_N^{1+}, (b) V_{Ga}^{3-}, (c) C_N^{1-}, and (d) C_N-Si_{Ga} point defect. Blue (red) color corresponds to occupied (unoccupied) states with the blue (red) shaded region corresponding to the pristine valence (conduction) band. Localized (defect) states are shown with dashed lines. Band diagrams are on the same energy scale and aligned with respect to their valence band maxima for ease of comparison. The lowest-energy transition between occupied and unoccupied states is shown. The ~0.1 eV variation in the bulk band gap between different defects is due to the introduction of the defect. (e) The imaginary part of the dielectric function for pristine GaN and GaN in the presence of the V_N^{1+}, V_{Ga}^{3-}, C_N^{1-}, and C_N-Si_{Ga} defects. A Gaussian broadening of 0.1 eV was applied and the spectra are normalized such that the highest peak in the energy window was set to 1. In the case of charged defects an electrostatic correction was applied to localized defect states as described in the text.

centered on nitrogen atoms. For V_{Ga}^{3-}, the hole is localized near the defect site with a radial expectation value of the charge density of 2.5 Å; the charge density associated with this state is centered mainly on three nitrogen atoms surrounding the gallium vacancy. For C_N^{1-}, the hole is centered near the defect site with a radial expectation value of 3.2 Å; the charge density

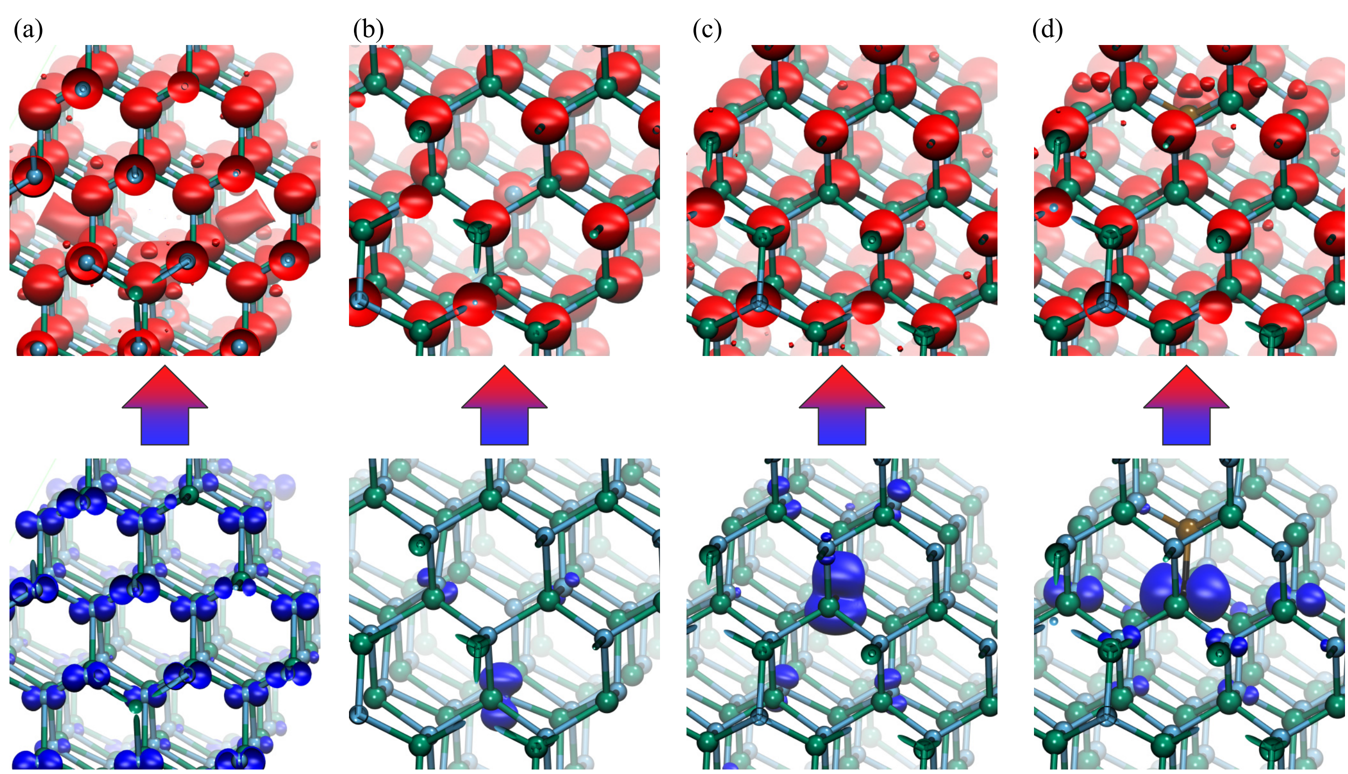

FIG. 5. The hole and electron density associated with the lowest-energy excited-state transition calculated within TDSRSH for the (a) V_N^{1+}, (b) V_{Ga}^{3-}, (c) C_N^{1-}, and (d) C_N-Si_{Ga} defects. The density is calculated as a weighted combination of transitions from Kohn-Sham orbitals. The lower plot shows the occupied hole state while the upper plot shows the unoccupied electron state. All isosurfaces enclose 30% of the respective charge distribution's total charge.

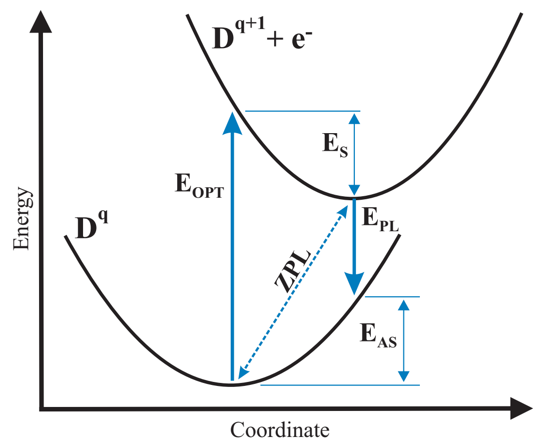

FIG. 6. A schematic of the configuration coordinate diagram showing the processes of photoabsorption and luminescence. Starting with a defect in the ground state D^q, in charge state q (bottom curve), an incident photon excites the material to state D^{q+1} (top curve) that has the same geometry as the ground state but a different defect charge state $q+1$, where the electron is now in the conduction band. The vertical shift in energy between the two systems is $E_{\rm opt}$ and is followed by a relaxation of the atoms to the minimum energy of D^{q+1}, shifted by the amount of the Stokes shift E_S. The transition back to the initial ground state occurs either without phonons at the energy of the zero-phonon line (ZPL) or via the multistep process involving return to state D^q and emission of a photon with energy $E_{\rm PL}$ followed by relaxation back to the equilibrium ground-state system, with energy change given by the anti-Stokes shift E_{AS}.

for this state is mainly centered on the carbon impurity, with some hole density on nearest-neighbor nitrogen atoms. For C_N-Si_{Ga}, the hole density is more delocalized with a radial expectation value of 4.2 Å and is centered mainly on the carbon impurity atom with some charge density at several nearest-neighbor nitrogen atoms, and no appreciable charge density on the silicon impurity.

C. Connection of calculations to YL in GaN

As noted in the Introduction, many studies compute the configuration coordinate diagram from DFT to describe the optical absorption and photoluminescence of defective materials, an example of which is shown in Fig. 6. This figure depicts the effective excitation of a defect in charge state q (bottom curve) within the material to a system with the defect in charge state $q+1$ and an electron in the bulk conduction band (top curve). The vertical transitions $E_{\rm opt}$ and $E_{\rm PL}$ correspond to the onset of optical absorption and the photoluminescence peak, respectively. The energies associated with the geometry relaxations are given by the Stokes (E_S) and anti-Stokes (E_{AS}) shifts. Within the ground-state DFT framework, the optical transition $E_{\rm opt}$ is calculated as total-energy differences between two charge states of a defect, and thus considers a defect-to-bulk transition without considering electron-hole interactions. Within this approximation, calculations based on the HSE functional have predicted $E_{\rm opt}$ of 3.78 eV for V_N^{1+} [125], 1.23 eV for V_{Ga}^{3-} [124], 2.95 eV for C_N^{1-} [19], and 3.57 eV for C_N-Si_{Ga} [22]; taking the same approximation, our calculations predict a value of 3.60, 1.27, 2.83, and 3.46 eV, respectively. For V_{Ga}^{3-}, C_N^{1-}, and C_N-Si_{Ga}, our predictions are within 0.12 eV of these previous studies, suggesting that these two different perspectives result in similar conclusions. The slightly larger discrepancy between our calculation and Ref. [125] for V_N^{1+} (0.18 eV) may be due to the use of different supercell sizes and the fact that we predict a bulklike excitation for V_N^{1+} (rather than bulk to defect) and so are not describing the same state. Given the relaxation energies calculated within DFT, Refs. [19,22,124,125] predict the photoluminescence peak $E_{\rm PL}$ to be located at 2.24 eV for V_N^{1+} [125], 0.25 eV for V_{Ga}^{3-} [124], 2.14 eV for C_N^{1-} [19], and 2.71 eV for C_N-Si_{Ga} [22], suggesting both V_N^{1+} and C_N^{1-} as potential sources of YL. However, based on the transient behavior observed in relatively recent PL experiments, V_N^{1+} is more likely to be associated with the GL2 band [95,125]. Based on calculated energetics, V_{Ga}^{3-} and C_N-Si_{Ga} are unlikely to be responsible for YL.

To better understand the C_N^{1-} defect as a possible source of YL, we further refine our calculations for this particular defect in GaN. TDSRSH provides the optical absorption onset $E_{\rm opt}$; in order to calculate $E_{\rm PL}$ in Fig. 6, it is necessary to include the Stokes shift associated with geometry reorganization due to the presence of electron and hole. Here, we approximate $E_{\rm PL}$ as the lowest-energy transition predicted by TDSRSH on C_N^{1-} in the ground-state geometry associated with removing an electron from the defect (i.e., C_N^0). We note that the exciton binding energy is included in this calculation whereas it is not included in the calculations of Lyons *et al.* discussed above [19] and that we have improved the k-point mesh to $8\times8\times8$ in order to better describe the exciton binding energies. $E_{\rm PL}$ calculated in this way is predicted to be 2.02 eV, in good agreement with Ref. [19]. Thus, we confirm that this defect may potentially cause the YL1 PL band of GaN, in agreement with these previously computed thermodynamic transition levels and measurements [96]. This is further validation that this (TD)SRSH approach can provide a new perspective on the optoelectronic properties of defective materials.

IV. CONCLUSION

In summary, we utilized a tuned and screened range-separated hybrid functional to describe the charged and neutral excited states of defective GaN, benchmarking the approach against *GW*/BSE. We tuned the functional to the pristine bulk GaN and applied it to a series of defective structures. For both the pristine material and one with a nitrogen vacancy in the 1+ charge state (V_N^{1+}), we determined that TDSRSH improves the agreement with *GW*/BSE when compared with TDHSE. Furthermore, we applied (TD)SRSH to a series of important point defects in GaN and found good agreement between our calculations and previous DFT-based studies of transition energies. For the point defects V_N^{1+}, V_{Ga}^{3-}, C_N^{1-}, and the complex C_N-Si_{Ga}, we predict defect-centered states either in the band gap or near band edges of GaN, which contribute to low-energy transitions in the optical spectrum. Additionally, by accounting for the Stokes shift, we predict that the C_N^{1-} vacancy is a candidate for the yellow luminescence in GaN, in agreement with previous theoretical calculations and recent measurements. Our study establishes the accuracy of TDSRSH for predicting the excited-state energetics of defective semiconductors, without making *a priori* assumptions about the nature of the transitions.

ACKNOWLEDGMENTS

The authors gratefully acknowledge Dr. M. Matsubara and Prof. E. Bellotti (Boston University) for providing their defective material structures and electrostatic corrections. We also acknowledge Professor R. Goldhahn (Otto von Guericke University) for providing the raw experimental data of the imaginary dielectric function of GaN, and D. Wing (Weizmann Institute of Science) for providing us the script to broaden the VASP-calculated TDDFT spectra. D.K.L and S.S. gratefully acknowledge funding from the U S Department of Energy (DOE), Office of Science, Basic Energy Sciences (BES) Early Career Program under Award No. DE-SC0018080. Additionally, we acknowledge grants of computer time from the National Energy Research Scientific Computing Center (NERSC), a DOE Office of Science User Facility supported by the Office of Science of the US Department of Energy under Contract No. DE-AC02-05CH11231, the Extreme Science and Engineering Discovery Environment (XSEDE), which is supported by National Science Foundation Grant No. ACI-1548562, and Boston University Scientific Computing Center at the Massachusetts Green High-Performance Computing Center (MGHPCC).

[1] H. J. Queisser and E. E. Haller, Defects in semiconductors: Some fatal, some vital, Science **281**, 945 (1998).

[2] W. Shockley and W. T. Read, Statistics of the recombinations of holes and electrons, Phys. Rev. **87**, 835 (1952).

[3] M. Grundmann, *The Physics of Semiconductors: An Introduction Including Nanophysics and Applications* (Springer, Heidelberg, 2015).

[4] S. Ghatak, A. N. Pal, and A. Ghosh, Nature of electronic states in atomically thin MoS_2 field-effect transistors, ACS Nano **5**, 7707 (2011).

[5] P. Dean and D. Herbert, Bound excitons in semiconductors, in *Excitons*, edited by K. Cho, Topics in Current Physics Vol. 14 (Springer, Berlin, 1979), Chap. 3, pp. 55–182.

[6] R. Laskowski, N. E. Christensen, G. Santi, and C. Ambrosch-Draxl, *Ab initio* calculations of excitons in GaN, Phys. Rev. B **72**, 035204 (2005).

[7] D. K. Lewis and S. Sharifzadeh, Defect-induced exciton localization in bulk gallium nitride from many-body perturbation theory, Phys. Rev. Mater. **3**, 114601 (2019).

[8] J. Zhu, T. D. dela Rubia, L. H. Yang, C. Mailhiot, and G. H. Gilmer, *Ab initio* pseudopotential calculations of B diffusion and pairing in Si, Phys. Rev. B **54**, 4741 (1996).

[9] C. G. Van de Walle, P. J. H. Denteneer, Y. Bar-Yam, and S. T. Pantelides, Theory of hydrogen diffusion and reactions in crystalline silicon, Phys. Rev. B **39**, 10791 (1989).

[10] J. Coutinho, R. Jones, P. R. Briddon, and S. Öberg, Oxygen and dioxygen centers in Si and Ge: Density-functional calculations, Phys. Rev. B **62**, 10824 (2000).

[11] P. Rinke, A. Janotti, M. Scheffler, and C. G. Van de Walle, Defect Formation Energies Without the Band-Gap Problem: Combining Density-Functional Theory and the *GW* Approach for the Silicon Self-Interstitial, Phys. Rev. Lett. **102**, 026402 (2009).

[12] D. J. Chadi and K. J. Chang, Theory of the Atomic and Electronic Structure of DX Centers in GaAs and $Al_xGa_{1-x}As$ Alloys, Phys. Rev. Lett. **61**, 873 (1988).

[13] J. Dabrowski and M. Scheffler, Theoretical Evidence for an Optically Inducible Structural Transition of the Isolated As Antisite in GaAs: Identification and Explanation of EL2? Phys. Rev. Lett. **60**, 2183 (1988).

[14] S. B. Zhang and J. E. Northrup, Chemical Potential Dependence of Defect Formation Energies in GaAs: Application to Ga Self-Diffusion, Phys. Rev. Lett. **67**, 2339 (1991).

[15] J. E. Northrup and S. B. Zhang, Dopant and defect energetics: Si in GaAs, Phys. Rev. B **47**, 6791 (1993).

[16] J. Neugebauer and C. G. Van de Walle, Atomic geometry and electronic structure of native defects in GaN, Phys. Rev. B **50**, 8067 (1994).

[17] C. G. Van de Walle, Interactions of hydrogen with native defects in GaN, Phys. Rev. B **56**, R10020 (1997).

[18] A. Stroppa and G. Kresse, Unraveling the Jahn-Teller effect in Mn-doped GaN using the Heyd-Scuseria-Ernzerhof hybrid functional, Phys. Rev. B **79**, 201201(R) (2009).

[19] J. L. Lyons, A. Janotti, and C. G. Van de Walle, Carbon impurities and the yellow luminescence in GaN, Appl. Phys. Lett. **97**, 152108 (2010).

[20] J. L. Lyons, A. Janotti, and C. G. Van de Walle, Shallow Versus Deep Nature of Mg Acceptors in Nitride Semiconductors, Phys. Rev. Lett. **108**, 156403 (2012).

[21] M. Matsubara and E. Bellotti, A first-principles study of carbon-related energy levels in GaN. I. Complexes formed by substitutional/interstitial carbons and gallium/nitrogen vacancies, J. Appl. Phys. **121**, 195701 (2017).

[22] M. Matsubara and E. Bellotti, A first-principles study of carbon-related energy levels in GaN. II. Complexes formed by carbon and hydrogen, silicon or oxygen, J. Appl. Phys. **121**, 195702 (2017).

[23] C. Freysoldt, B. Grabowski, T. Hickel, J. Neugebauer, G. Kresse, A. Janotti, and C. G. Van de Walle, First-principles calculations for point defects in solids, Rev. Mod. Phys. **86**, 253 (2014).

[24] F. Oba and Y. Kumagai, Design and exploration of semiconductors from first principles: A review of recent advances, Appl. Phys. Express **11**, 060101 (2018).

[25] A. Gali, Time-dependent density functional study on the excitation spectrum of point defects in semiconductors, Phys. Status Solidi B **248**, 1337 (2011).

[26] C. E. Dreyer, A. Alkauskas, J. L. Lyons, A. Janotti, and C. G. Van de Walle, First-principles calculations of point defects for quantum technologies, Annu. Rev. Mater. Res. **48**, 1 (2018).

[27] A. Alkauskas, B. B. Buckley, D. D. Awschalom, and C. G. V. de Walle, First-principles theory of the luminescence lineshape for the triplet transition in diamond NV centres, New J. Phys. **16**, 073026 (2014).

[28] A. Gali, E. Janzén, P. Deák, G. Kresse, and E. Kaxiras, Theory of Spin-Conserving Excitation of the $N-V^-$ Center in Diamond, Phys. Rev. Lett. **103**, 186404 (2009).

[29] M. L. Tiago and J. R. Chelikowsky, Optical excitations in organic molecules, clusters, and defects studied by first-principles Green's function methods, Phys. Rev. B **73**, 205334 (2006).
[30] L.-Y. Huang, X. Zhang, M. Zhang, and G. Lu, Effect of point defects on optical properties of graphene fluoride: A first-principles study, J. Phys. Chem. C **121**, 12855 (2017).
[31] J. Bang, S. Meng, and S. B. Zhang, Dynamic defect as nonradiative recombination center in semiconductors, Phys. Rev. B **100**, 245208 (2019).
[32] G. Onida, L. Reining, and A. Rubio, Electronic excitations: Density-functional versus many-body Green's-function approaches, Rev. Mod. Phys. **74**, 601 (2002).
[33] L. Hedin, New method for calculating the one-particle Green's function with application to the electron-gas problem, Phys. Rev. **139**, A796 (1965).
[34] L. Hedin and S. Lundqvist, Effects of electron-electron and electron-phonon interactions on the one-electron states of solids, Solid State Phys. **23**, 1 (1970).
[35] M. S. Hybertsen and S. G. Louie, First-Principles Theory of Quasiparticles: Calculation of Band Gaps in Semiconductors and Insulators, Phys. Rev. Lett. **55**, 1418 (1985).
[36] M. S. Hybertsen and S. G. Louie, Electron correlation in semiconductors and insulators: Band gaps and quasiparticle energies, Phys. Rev. B **34**, 5390 (1986).
[37] F. Aryasetiawan and O. Gunnarsson, The *GW* method, Rep. Prog. Phys. **61**, 237 (1998).
[38] G. Stefanucci and R. van Leeuwen, *Nonequilibrium Many-Body Theory of Quantum Systems: A Modern Introduction* (Cambridge University Press, Cambridge, 2013).
[39] R. M. Martin, L. Reining, and D. M. Ceperley, *Interacting Electrons* (Cambridge University Press, New York, 2016).
[40] G. Strinati, Application of the Green's functions method to the study of the optical properties of semiconductors, Riv. Nuovo Cimento Ser. 3 **11**, 1 (1988).
[41] M. Rohlfing and S. G. Louie, Electron-hole excitations and optical spectra from first principles, Phys. Rev. B **62**, 4927 (2000).
[42] M. P. Surh, H. Chacham, and S. G. Louie, Quasiparticle excitation energies for the F-center defect in LiCl, Phys. Rev. B **51**, 7464 (1995).
[43] M. Bockstedte, A. Marini, O. Pankratov, and A. Rubio, Many-Body Effects in the Excitation Spectrum of a Defect in SiC, Phys. Rev. Lett. **105**, 026401 (2010).
[44] Y. Ma and M. Rohlfing, Optical excitation of deep defect levels in insulators within many-body perturbation theory: The *F* center in calcium fluoride, Phys. Rev. B **77**, 115118 (2008).
[45] Y. Ma, M. Rohlfing, and A. Gali, Excited states of the negatively charged nitrogen-vacancy color center in diamond, Phys. Rev. B **81**, 041204(R) (2010).
[46] C. Attaccalite, M. Bockstedte, A. Marini, A. Rubio, and L. Wirtz, Coupling of excitons and defect states in boron-nitride nanostructures, Phys. Rev. B **83**, 144115 (2011).
[47] M. Giantomassi, M. Stankovski, R. Shaltaf, M. Grüning, F. Bruneval, P. Rinke, and G.-M. Rignanese, Electronic properties of interfaces and defects from many-body perturbation theory: Recent developments and applications, Phys. Status Solidi B **248**, 275 (2011).
[48] M. Jain, J. R. Chelikowsky, and S. G. Louie, Quasiparticle Excitations and Charge Transition Levels of Oxygen Vacancies in Hafnia, Phys. Rev. Lett. **107**, 216803 (2011).
[49] S. Choi, M. Jain, and S. G. Louie, Mechanism for optical initialization of spin in NV^- center in diamond, Phys. Rev. B **86**, 041202(R) (2012).
[50] J. Lischner, J. Deslippe, M. Jain, and S. G. Louie, First-Principles Calculations of Quasiparticle Excitations of Open-Shell Condensed Matter Systems, Phys. Rev. Lett. **109**, 036406 (2012).
[51] P. Rinke, A. Schleife, E. Kioupakis, A. Janotti, C. Rödl, F. Bechstedt, M. Scheffler, and C. G. Van de Walle, First-Principles Optical Spectra for *F* Centers in MgO, Phys. Rev. Lett. **108**, 126404 (2012).
[52] S. Jiang, T. Lu, Y. Long, and J. Chen, *Ab initio* many-body study of the electronic and optical properties of $MgAl_2O_4$ spinel, J. Appl. Phys. **111**, 043516 (2012).
[53] N. Richard, L. Martin-Samos, S. Girard, A. Ruini, A. Boukenter, Y. Ouerdane, and J.-P. Meunier, Oxygen deficient centers in silica: Optical properties within many-body perturbation theory, J. Phys.: Condens. Matter **25**, 335502 (2013).
[54] A. Malashevich, M. Jain, and S. G. Louie, First-principles DFT + *GW* study of oxygen vacancies in rutile TiO_2, Phys. Rev. B **89**, 075205 (2014).
[55] W. Chen and A. Pasquarello, First-principles determination of defect energy levels through hybrid density functionals and *GW*, J. Phys.: Condens. Matter **27**, 133202 (2015).
[56] M. A. Flores, Defect properties of Sn- and Ge-doped ZnTe: Suitability for intermediate-band solar cells, Semicond. Sci. Technol. **33**, 015004 (2017).
[57] C. E. Ekuma, Effects of vacancy defects on the electronic and optical properties of monolayer PbSe, J. Phys. Chem. Lett. **9**, 3680 (2018).
[58] C. E. Ekuma and D. Gunlycke, Optical absorption in disordered monolayer molybdenum disulfide, Phys. Rev. B **97**, 201414(R) (2018).
[59] J. Jiang, R. Pachter, and S. Mou, Tunability in the optical response of defective monolayer WSe_2 by computational analysis, Nanoscale **10**, 13751 (2018).
[60] S. Refaely-Abramson, D. Y. Qiu, S. G. Louie, and J. B. Neaton, Defect-Induced Modification of Low-Lying Excitons and Valley Selectivity in Monolayer Transition Metal Dichalcogenides, Phys. Rev. Lett. **121**, 167402 (2018).
[61] S. Barja, S. Refaely-Abramson, B. Schuler, D. Y. Qiu, A. Pulkin, S. Wickenburg, H. Ryu, M. M. Ugeda, C. Kastl, C. Chen, C. Hwang, A. Schwartzberg, S. Aloni, S. K. Mo, D. Frank Ogletree, M. F. Crommie, O. V. Yazyev, S. G. Louie, J. B. Neaton, and A. Weber-Bargioni, Identifying substitutional oxygen as a prolific point defect in monolayer transition metal dichalcogenides, Nat. Commun. **10**, 3382 (2019).
[62] Y. J. Zheng, Y. Chen, Y. L. Huang, P. K. Gogoi, M.-Y. Li, L.-J. Li, P. E. Trevisanutto, Q. Wang, S. J. Pennycook, A. T. S. Wee, and S. Y. Quek, Point defects and localized excitons in 2D WSe_2, ACS Nano **13**, 6050 (2019).
[63] B. G. Janesko, T. M. Henderson, and G. E. Scuseria, Screened hybrid density functionals for solid-state chemistry and physics, Phys. Chem. Chem. Phys. **11**, 443 (2009).

[64] J. Heyd, G. E. Scuseria, and M. Ernzerhof, Erratum: Hybrid functionals based on a screened Coulomb potential [J. Chem. Phys. **118**, 8207 (2003)], J. Chem. Phys. **124**, 219906 (2006).
[65] J. P. Perdew, M. Ernzerhof, and K. Burke, Rationale for mixing exact exchange with density functional approximations, J. Chem. Phys. **105**, 9982 (1996).
[66] T. Yanai, D. P. Tew, and N. C. Handy, A new hybrid exchangecorrelation functional using the coulomb-attenuating method (CAM-B3LYP), Chem. Phys. Lett. **393**, 51 (2004).
[67] S. Botti, F. Sottile, N. Vast, V. Olevano, L. Reining, H.-C. Weissker, A. Rubio, G. Onida, R. Del Sole, and R. W. Godby, Long-range contribution to the exchange-correlation kernel of time-dependent density functional theory, Phys. Rev. B **69**, 155112 (2004).
[68] S. Sharma, J. K. Dewhurst, A. Sanna, and E. K. U. Gross, Bootstrap Approximation for the Exchange-Correlation Kernel of Time-Dependent Density-Functional Theory, Phys. Rev. Lett. **107**, 186401 (2011).
[69] S. Refaely-Abramson, S. Sharifzadeh, M. Jain, R. Baer, J. B. Neaton, and L. Kronik, Gap renormalization of molecular crystals from density-functional theory, Phys. Rev. B **88**, 081204(R) (2013).
[70] S. Refaely-Abramson, M. Jain, S. Sharifzadeh, J. B. Neaton, and L. Kronik, Solid-state optical absorption from optimally tuned time-dependent range-separated hybrid density functional theory, Phys. Rev. B **92**, 081204(R) (2015).
[71] Z.-h. Yang, F. Sottile, and C. A. Ullrich, Simple screened exact-exchange approach for excitonic properties in solids, Phys. Rev. B **92**, 035202 (2015).
[72] M. Gerosa, C. E. Bottani, C. D. Valentin, G. Onida, and G. Pacchioni, Accuracy of dielectric-dependent hybrid functionals in the prediction of optoelectronic properties of metal oxide semiconductors: A comprehensive comparison with many-body *GW* and experiments, J. Phys.: Condens. Matter **30**, 044003 (2017).
[73] W. Chen, G. Miceli, G.-M. Rignanese, and A. Pasquarello, Nonempirical dielectric-dependent hybrid functional with range separation for semiconductors and insulators, Phys. Rev. Mater. **2**, 073803 (2018).
[74] J. H. Skone, M. Govoni, and G. Galli, Self-consistent hybrid functional for condensed systems, Phys. Rev. B **89**, 195112 (2014).
[75] S. Rigamonti, S. Botti, V. Veniard, C. Draxl, L. Reining, and F. Sottile, Estimating Excitonic Effects in the Absorption Spectra of Solids: Problems and Insight from a Guided Iteration Scheme, Phys. Rev. Lett. **114**, 146402 (2015).
[76] J. H. Skone, M. Govoni, and G. Galli, Nonempirical range-separated hybrid functionals for solids and molecules, Phys. Rev. B **93**, 235106 (2016).
[77] N. P. Brawand, M. Vörös, M. Govoni, and G. Galli, Generalization of Dielectric-Dependent Hybrid Functionals to Finite Systems, Phys. Rev. X **6**, 041002 (2016).
[78] T. Shimazaki and Y. Asai, First principles band structure calculations based on self-consistent screened Hartree-Fock exchange potential, J. Chem. Phys. **130**, 164702 (2009).
[79] D. Wing, J. B. Haber, R. Noff, B. Barker, D. A. Egger, A. Ramasubramaniam, S. G. Louie, J. B. Neaton, and L. Kronik, Comparing time-dependent density functional theory with many-body perturbation theory for semiconductors: Screened range-separated hybrids and the *GW* plus Bethe-Salpeter approach, Phys. Rev. Mater. **3**, 064603 (2019).
[80] G. Miceli, W. Chen, I. Reshetnyak, and A. Pasquarello, Nonempirical hybrid functionals for band gaps and polaronic distortions in solids, Phys. Rev. B **97**, 121112(R) (2018).
[81] J. Sun, J. Yang, and C. A. Ullrich, Low-cost alternatives to the Bethe-Salpeter equation: Towards simple hybrid functionals for excitonic effects in solids, Phys. Rev. Res. **2**, 013091 (2020).
[82] J. P. Perdew, W. Yang, K. Burke, Z. Yang, E. K. U. Gross, M. Scheffler, G. E. Scuseria, T. M. Henderson, I. Y. Zhang, A. Ruzsinszky, H. Peng, J. Sun, E. Trushin, and A. Görling, Understanding band gaps of solids in generalized Kohn–Sham theory, Proc. Natl. Acad. Sci. USA **114**, 2801 (2017).
[83] L. Kronik and J. B. Neaton, Excited-state properties of molecular solids from first principles, Annu. Rev. Phys. Chem. **67**, 587 (2016).
[84] A. K. Manna, S. Refaely-Abramson, A. M. Reilly, A. Tkatchenko, J. B. Neaton, and L. Kronik, Quantitative prediction of optical absorption in molecular solids from an optimally tuned screened range-separated hybrid functional, J. Chem. Theory Comput. **14**, 2919 (2018).
[85] A. Ramasubramaniam, D. Wing, and L. Kronik, Transferable screened range-separated hybrids for layered materials: The cases of MoS_2 and h-BN, Phys. Rev. Mater. **3**, 084007 (2019).
[86] X. Zhang, G. Lu, R. Baer, E. Rabani, and D. Neuhauser, Linear-response time-dependent density functional theory with stochastic range-separated hybrids, J. Chem. Theory Comput. **16**, 1064 (2020).
[87] M. A. Reshchikov, Point defects in GaN, in *Defects in Semiconductors*, edited by L. Romano, V. Privitera, and C. Jagadish, Semiconductors and Semimetals Vol. 91 (Elsevier, Boston, 2015), Chap. 9, pp. 315–367.
[88] S. Pimputkar, Gallium nitride, in *Single Crystals of Electronic Materials*, edited by R. Fornari, Woodhead Publishing Series in Electronic and Optical Materials (Woodhead Publishing, Cambridge, 2019), Chap. 11, pp. 351–399.
[89] Z. Xie, Y. Sui, J. Buckeridge, C. R. A. Catlow, T. W. Keal, P. Sherwood, A. Walsh, M. R. Farrow, D. O. Scanlon, S. M. Woodley, and A. A. Sokol, Donor and acceptor characteristics of native point defects in GaN, J. Phys. D: Appl. Phys. **52**, 335104 (2019).
[90] T. Ogino and M. Aoki, Mechanism of yellow luminescence in GaN, Jpn. J. Appl. Phys. **19**, 2395 (1980).
[91] J. Neugebauer and C. G. Van de Walle, Gallium vacancies and the yellow luminescence in GaN, Appl. Phys. Lett. **69**, 503 (1996).
[92] A. Alkauskas, J. L. Lyons, D. Steiauf, and C. G. Van de Walle, First-Principles Calculations of Luminescence Spectrum Line Shapes for Defects in Semiconductors: The Example of GaN and ZnO, Phys. Rev. Lett. **109**, 267401 (2012).
[93] P. Shah, R. Dedhia, R. Tompkins, E. Viveiros, and K. Jones, DLTS and MCTS analysis of the influence of growth pressure on trap generation in MOCVD GaN, Solid-State Electron. **78**, 121 (2012).
[94] Q. Yan, A. Janotti, M. Scheffler, and C. G. Van de Walle, Role of nitrogen vacancies in the luminescence of Mg-doped GaN, Appl. Phys. Lett. **100**, 142110 (2012).

[95] M. A. Reshchikov, D. O. Demchenko, J. D. McNamara, S. Fernández-Garrido, and R. Calarco, Green luminescence in Mg-doped GaN, Phys. Rev. B **90**, 035207 (2014).
[96] M. A. Reshchikov, M. Vorobiov, D. O. Demchenko, Ü. Özgür, H. Morkoç, A. Lesnik, M. P. Hoffmann, F. Hörich, A. Dadgar, and A. Strittmatter, Two charge states of the C_N acceptor in GaN: Evidence from photoluminescence, Phys. Rev. B **98**, 125207 (2018).
[97] G. Kresse and J. Furthmüller, Efficient iterative schemes for *ab initio* total-energy calculations using a plane-wave basis set, Phys. Rev. B **54**, 11169 (1996).
[98] P. E. Blöchl, Projector augmented-wave method, Phys. Rev. B **50**, 17953 (1994).
[99] D. K. Lewis, M. Matsubara, E. Bellotti, and S. Sharifzadeh, Quasiparticle and hybrid density functional methods in defect studies: An application to the nitrogen vacancy in GaN, Phys. Rev. B **96**, 235203 (2017).
[100] O. Lagerstedt and B. Monemar, Variation of lattice parameters in GaN with stoichiometry and doping, Phys. Rev. B **19**, 3064 (1979).
[101] J. Heyd, G. E. Scuseria, and M. Ernzerhof, Hybrid functionals based on a screened coulomb potential, J. Chem. Phys. **118**, 8207 (2003).
[102] B. Monemar, Fundamental energy gap of GaN from photoluminescence excitation spectra, Phys. Rev. B **10**, 676 (1974).
[103] H. J. Monkhorst and J. D. Pack, Special points for Brillouin-zone integrations, Phys. Rev. B **13**, 5188 (1976).
[104] G. Makov, R. Shah, and M. C. Payne, Periodic boundary conditions in *ab initio* calculations. II. Brillouin-zone sampling for aperiodic systems, Phys. Rev. B **53**, 15513 (1996).
[105] N. Marzari, A. A. Mostofi, J. R. Yates, I. Souza, and D. Vanderbilt, Maximally localized Wannier functions: Theory and applications, Rev. Mod. Phys. **84**, 1419 (2012).
[106] A. A. Mostofi, J. R. Yates, G. Pizzi, Y.-S. Lee, I. Souza, D. Vanderbilt, and N. Marzari, An updated version of wannier90: A tool for obtaining maximally-localised Wannier functions, Comput. Phys. Commun. **185**, 2309 (2014).
[107] S. L. Adler, Quantum theory of the dielectric constant in real solids, Phys. Rev. **126**, 413 (1962).
[108] N. Wiser, Dielectric constant with local field effects included, Phys. Rev. **129**, 62 (1963).
[109] M. Gajdoš, K. Hummer, G. Kresse, J. Furthmüller, and F. Bechstedt, Linear optical properties in the projector-augmented wave methodology, Phys. Rev. B **73**, 045112 (2006).
[110] M. E. Casida, Time-dependent density functional response theory for molecules, in *Recent Advances in Density Functional Methods*, edited by D. P. Chong (World Scientific, Singapore, 1995), pp. 155–192.
[111] J. Deslippe, G. Samsonidze, D. A. Strubbe, M. Jain, M. L. Cohen, and S. G. Louie, BerkeleyGW: A massively parallel computer package for the calculation of the quasiparticle and optical properties of materials and nanostructures, Comput. Phys. Commun. **183**, 1269 (2012).
[112] P. Giannozzi, S. Baroni, N. Bonini, M. Calandra, R. Car, C. Cavazzoni, D. Ceresoli, G. L. Chiarotti, M. Cococcioni, I. Dabo, A. D. Corso, S. de Gironcoli, S. Fabris, G. Fratesi, R. Gebauer, U. Gerstmann, C. Gougoussis, A. Kokalj, M. Lazzeri, L. Martin-Samos *et al.*, QUANTUM ESPRESSO: A modular and open-source software project for quantum simulations of materials, J. Phys.: Condens. Matter **21**, 395502 (2009).
[113] W. Chen and A. Pasquarello, Correspondence of defect energy levels in hybrid density functional theory and many-body perturbation theory, Phys. Rev. B **88**, 115104 (2013).
[114] C. Freysoldt, J. Neugebauer, and C. G. Van de Walle, Fully *ab Initio* Finite-Size Corrections for Charged-Defect Supercell Calculations, Phys. Rev. Lett. **102**, 016402 (2009).
[115] C. Freysoldt, J. Neugebauer, and C. G. Van de Walle, Electrostatic interactions between charged defects in supercells, Phys. Status Solidi B **248**, 1067 (2011).
[116] See Supplemental Material at http://link.aps.org/supplemental/10.1103/PhysRevMaterials.4.063803 for a description of how the electrostatic correction was applied to the wave-function file, details on the determination of the geometrical center of a defect wave function for use in calculating $\langle r\rangle$ from Eq. (2), and a comparison of defect-state energies obtained using the *GW* approach and DFT with the HSE and SRSH functionals.
[117] C. W. M. Castleton, A. Höglund, and S. Mirbt, Density functional theory calculations of defect energies using supercells, Modell. Simul. Mater. Sci. Eng. **17**, 084003 (2009).
[118] M. Feneberg, M. F. Romero, M. Röppischer, C. Cobet, N. Esser, B. Neuschl, K. Thonke, M. Bickermann, and R. Goldhahn, Anisotropic absorption and emission of bulk **$(1\bar{1}00)$** AlN, Phys. Rev. B **87**, 235209 (2013).
[119] W. Setyawan and S. Curtarolo, High-throughput electronic band structure calculations: Challenges and tools, Comput. Mater. Sci. **49**, 299 (2010).
[120] S. J. Xu, W. Liu, and M. F. Li, Direct determination of free exciton binding energy from phonon-assisted luminescence spectra in GaN epilayers, Appl. Phys. Lett. **81**, 2959 (2002).
[121] J. Paier, M. Marsman, and G. Kresse, Dielectric properties and excitons for extended systems from hybrid functionals, Phys. Rev. B **78**, 121201(R) (2008).
[122] M. Dvorak, S.-H. Wei, and Z. Wu, Origin of the Variation of Exciton Binding Energy in Semiconductors, Phys. Rev. Lett. **110**, 016402 (2013).
[123] R. Gillen and J. Robertson, A hybrid density functional view of native vacancies in gallium nitride, J. Phys.: Condens. Matter **25**, 405501 (2013).
[124] J. L. Lyons, A. Alkauskas, A. Janotti, and C. G. Van de Walle, First-principles theory of acceptors in nitride semiconductors, Phys. Status Solidi B **252**, 900 (2015).
[125] I. C. Diallo and D. O. Demchenko, Native Point Defects in GaN: A Hybrid-Functional Study, Phys. Rev. Applied **6**, 064002 (2016).